Theoretical Study of Inhibition of Adenosine Deaminase by (8*R*)-Coformycin and (8*R*)-Deoxycoformycin

Tami J. Marrone,*,† T. P. Straatsma,‡ James M. Briggs,† David K. Wilson,§ Florante A. Quiocho,§ and J. Andrew McCammon†

Departments of Chemistry and Biochemistry and of Pharmacology, University of California, San Diego, La Jolla, California 92093-0365, Pacific Northwest Laboratories, Battelle Boulevard, Richland, Washington 99352, and Department of Biochemistry and Howard Hughes Medical Institute, Baylor College of Medicine, Houston, Texas 77030

Received July 31, 1995[⊗]

Molecular dynamics and free energy simulations were performed to examine the binding of (8*R*)-deoxycoformycin and (8*R*)-coformycin to adenosine deaminase. The two inhibitors differ only at the 2′ position of the sugar ring; the sugar moiety of conformycin is ribose, while it is deoxyribose for deoxycoformycin. The 100 ps molecular dynamics trajectories reveal that Asp 19 and His 17 interact strongly with the 5′ hydroxyl group of the sugar moiety of both inhibitors and appear to play an important role in binding the sugar. The 2′ and 3′ groups of the sugars are near the protein−water interface and can be stabilized by either protein residues or water. The flexibility of the residues at the opening of the active site helps to explain the modest difference in binding of the two inhibitors and how substrates/inhibitors can enter an otherwise inaccessible binding site.

Introduction

Adenosine deaminase (ADA) is of great interest to the medical community because of its role in certain lymphomas, leukemias, and diseases of the immune system, particularly, severe combined immunodeficiency disease.[1] Inhibition of this enzyme has been shown to be an effective treatment for some of these immunological disorders.[2] ADA hydrolytically deaminates adenosine to form inosine and ammonia and can hydrolyze the substituent of the 6 position of a variety of substituted purine nucleosides. The enzyme's hydrolytic capabilities have been exploited to convert lipophilic 6-substituted purine nucleosides to products which show anti-HIV (human immunodeficiency virus) activity.[3,4] The lipophilic nature of the substrates could allow them to cross the blood−brain barrier and treat the HIV virus in the central nervous system.[3,4]

Understanding the interaction of ADA with its inhibitors and its substrates at the molecular level will be important in the development of the next generation of pharmaceutical agents that act as inhibitors or substrates. Computer simulations can examine these interactions at the molecular level and describe features important for ADA−substrate and ADA−inhibitor recognition. In this paper we describe the simulation of (8*R*)-coformycin and (8*R*)-deoxycoformycin (referred to as coformycin and deoxycoformycin throughout the rest of the paper), which are potent inhibitors of ADA with K_i values of 1×10^{-11} and 2.5×10^{-12} M, respectively.[5,6] The two molecules differ only at the 2′ position of the sugar ring; the sugar moiety of coformycin is ribose, while it is deoxyribose for deoxycoformycin. A schematic diagram of these inhibitors is shown in Figure 1. The sugar could play an important role in the binding process for transition state analogues such as coformycin and deoxycoformycin. Experimental studies show that the binding affinity of 1,6-dihydro-6-(hydroxyethyl)purine ribonucleoside, a transition state analogue, is reduced by orders of magnitude when the ribose is replaced with a hydrogen as the 9 substituent.[7]

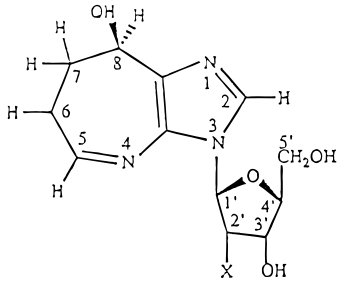

Figure 1. Schematic diagram of the ADA inhibitors (8*R*)-deoxycoformycin (X = H) and (8*R*)-coformycin (X = OH).

Recently, the structure of ADA with deoxycoformycin bound in the active site has been solved by Wilson and Quiocho,[8] and a stereoview of active site residues is shown in Figure 2. The zinc is coordinated by the ϵ nitrogens (Nϵ2) of the His 15, His 17, and His 214, by a carboxylate oxygen (Oδ2) of Asp 295, and the hydroxyl oxygen (8-OH) of the deoxycoformycin inhibitor. This structure is very similar to the structure published by Wilson et al., with 6-hydroxypurine riboside (HDPR) bound in the active site. The HDPR structure by Wilson et al.[9] was the first structure solved for ADA and the first to demonstrate the existence of a zinc ion in the active site. The zinc ion in the HDPR structure is coordinated by the aforementioned aspartate and histidines as well as by the 6-OH from the HDPR.

Molecular dynamics (MD) and free energy simulations of coformycin and deoxycoformycin and their complexes with ADA can be used to obtain structural and dynamic insights into the behavior of these molecules and to help understand the differences in the strength of binding of these inhibitors. In particular, free energy simulations can provide the relative free energy of binding of inhibitors. In order to investigate the binding properties of these inhibitors using MD and free energy techniques, a theoretical model was developed for the enzyme and the inhibitors. Thus, the parametrization of the models

† University of California, San Diego.
‡ Pacific Northwest Laboratories.
§ Baylor College of Medicine.
[⊗] Abstract published in *Advance ACS Abstracts,* November 15, 1995.

0022-2623/96/1839-0277$12.00/0

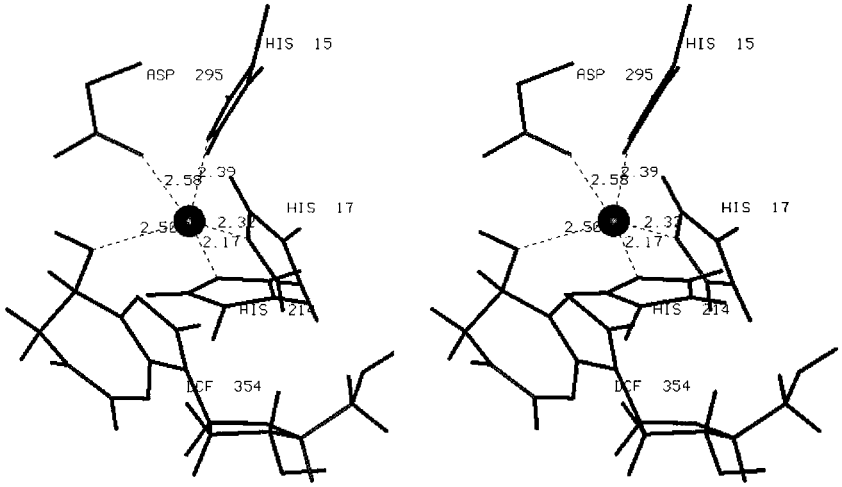

Figure 2. Stereoview of the zinc and its ligands in the active site of the ADA/deoxycoformycin crystal structure.

used to represent this system will be discussed first. Next, the computational procedure will be described followed by a discussion of the energetic and structural results from the simulations. Finally, conclusions will be drawn from the simulation results.

Parametrization

Point charges for the zinc-centered active site of ADA were determined from high-level *ab initio* calculations using the Gaussian92 series of programs.[10] A reduced model for the acitve site was chosen so that the calculation was tractable. This model included imidazoles in place of the three histidines (His 15, 17, and 214), an acetate for the aspartate (Asp 295), and deoxycoformycin without the 2′-deoxyribose ring. A double-ζ basis set[11] was used for all atoms of the zinc ligands. This was augmented with a set of *d*-functions on the non-hydrogen centers to help represent the polarization of the electron clouds due to the presence of the zinc ion. A Hay−Wadt effective core potential was used for the 18 core electrons in zinc along with the appropriate double-ζ basis set for the valence electrons.[12] A single-point energy calculation was performed, with the atoms in the locations specified by the crystal structure, to obtain a high-level wave function. The CHELPG[13] fitting procedure was used within Gaussian92 to obtain a set of atom-centered charges for the model of the ADA active site; a radius of 1.25 Å was used for the zinc ion. Charges for the purine analogue ring, used in free energy simulations of the free inhibitor in solution, were obtained from a 6-31G* single-point energy calculation in Gaussian92[10] using the CHELPG[13] fitting procedure.

The Lennard−Jones terms for the zinc-bound amino acid residues were taken from the OPLS force field for amino acids, while the Lennard−Jones parameters for zinc were taken from the Hoops et al. force field for human carbonic anhydrase II.[14] The bond, angle, and dihedral parameters involving the zinc and its ligands were adapted from the Hoops et al.[14] force field with some modifications and are presented as supporting information. Appropriate Lennard−Jones terms were extracted from the BOSS 31[15] parameter file to describe the deoxycoformycin ring. The nonbonded parameters (charges and Lennard−Jones terms) for the ribose and 2′-deoxyribose were taken from the BOSS 31[15] parameter file. OPLS[16] nonbonded terms and AMBER[17] bonded terms were used to describe the rest of the protein. The deoxycoformycin (DCF) and coformycin (CF) molecules were all-atom models in the simulations. The active site residue side chains and Phe and Tyr side chains were also represented as all-atom models,[18] while the rest of the protein residues were represented as united atom models. Phe and Tyr are represented as all-atom because Phe and Tyr residues were near the point of perturbation, and it was desired to represent the detailed charge distributions of these aromatic side chains. The 1−4 scaling factor for the Lennard−Jones interactions was increased from $^1/_8$ to 1 for polar pairs to avoid tight 1−5 intramolecular hydrogen bonds.[19] The 1−4 scaling factor for the Lennard−Jones interactions remained $^1/_8$ for all other 1−4 pairs, and the electrostatic scaling factor remained $^1/_2$ for all 1−4 pairs. The ionization states were calculated via the method of Antosiowicz et al.[20] using UHBD.[21] The ionization states of the residues of ADA that differ from the predicted ionization states of the free amino acids at pH 7.0 are given in Table 1.

Table 1. Calculated Ionization States for Residues of ADA That Differ from Predicted Ionization States of the Free Amino Acids at pH 7.0

residue	ionization state
His 105	+1
His 197	+1
His 210	+1
His 238	+1
His 241	+1

Computational Methods

The relative free energy of binding can be determined via the thermodynamic cycle below:[22]

$$\begin{array}{ccccc} & & & \xrightarrow{\Delta A_1} & \\ \text{ADA} & + & \text{DCF} & & \text{ADA·DCF} \\ & \Delta A_3 \downarrow & & & \downarrow \Delta A_4 \\ \text{ADA} & + & \text{CF} & \xrightarrow[\Delta A_2]{} & \text{ADA·CF} \end{array}$$

$$\Delta\Delta A = \Delta A_2 - \Delta A_1 = \Delta A_4 - \Delta A_3 \quad (1)$$

Rather than calculate the horizontal processes of the thermodynamic cycle at great computational expense, the vertical processes can be calculated and used to determine the relative free energies of binding. Here the parameters that describe DCF are perturbed into the parameters that describe

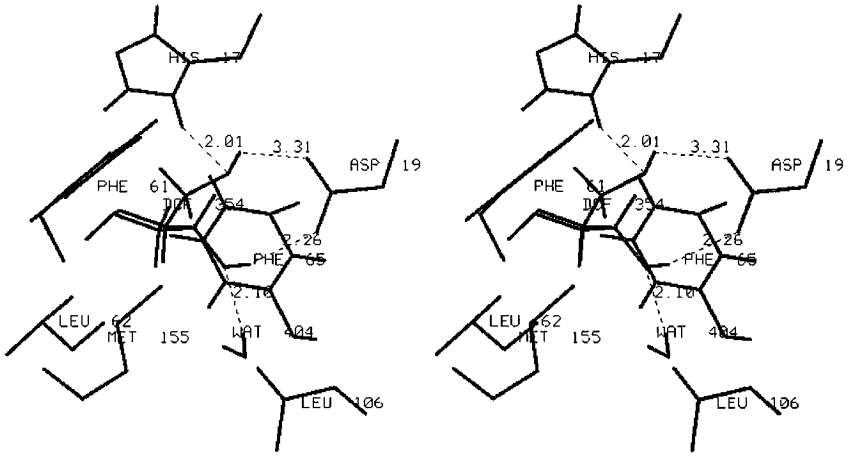

Figure 3. Stereoview of all residues within 6 Å of C2′ or C3′ of deoxycoformycin in the crystal structure.

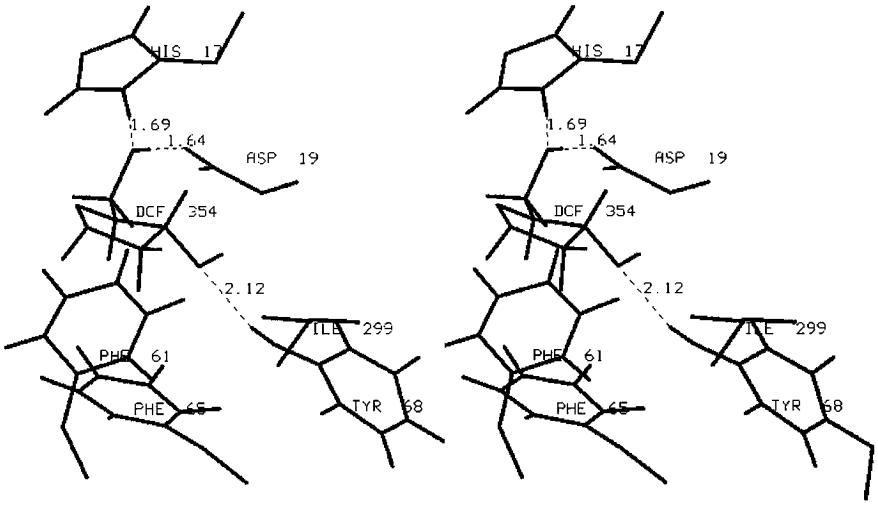

Figure 4. Stereoview of the active site after equilibration. All residues within 6 Å of C2′ or C3′ are shown.

CF in both the enzyme and solution. This type of calculation determines which inhibitor binds more tightly to the enzyme. One method for doing this type of simulation is multiconfiguration thermodynamic integration (MCTI)[23] which is based on eq 2:

$$\Delta A = \int \left\langle \left(\frac{\partial H}{\partial \lambda} \right)_{T,V} \right\rangle_{\lambda} d\lambda \qquad (2)$$

Here, A is the Helmholtz free energy, H is the Hamiltonian of the system, and λ is a parameter that describes the composition of the system. As one inhibitor ($\lambda = 0$) is perturbed into another inhibitor ($\lambda = 1$), the ensemble average of the derivative is calculated and integrated over the perturbation.

Protein/Inhibitor. All simulations were performed with the ARGOS[24] program. The initial coordinates for the ADA/DCF complex and its 50 crystal waters were taken from the crystal structure.[8] Missing polar hydrogens were added to the structure. The complex was placed in a cubic box of SPC/E[25] water molecules with a box length of 85 Å on each side. Water molecules whose centers were closer than 2.5 Å to a heavy atom of the complex were deleted. Initially, all nonbonded cutoffs were set to 5 Å due to the large size of the system and the use of periodic boundary conditions. The periodic boundary conditions were combined with coupling to a pressure bath to obtain the correct solvent density. All hydrogens on the enzyme and inhibitor were relaxed for 250 steps of steepest descent while the remainder of the system remained fixed. The water was relaxed for 250 steps of steepest descent minimization and then thermalized for 20 ps at 300 K via MD with a time step of 2 fs, with velocity reassignment every 0.2 ps, while the protein remained fixed. The protein was then relaxed for 250 steps of steepest descent while the water remained fixed. At this point, a sphere was cut from the box with a 32 Å radius centered at the point of perturbation (C2′ of the sugar), and the periodic boundary conditions were removed. To continue the equilibration, constraints were applied to the system such that all protein charge groups at distances beyond 20 Å from the point of perturbation and all water molecules were fixed. The nonbonded cutoff was increased to 9 Å (short range) and 12 Å (long range). The protein was then thermalized using velocity reassignment with the following schedule: 5 ps at 100 K, 5 ps at 200 K, and 5 ps at 300 K. Constraints were removed from the water molecules within 20 Å of the point of perturbation. Thus all groups within the 20 Å radius were unconstrained, and all groups outside the 20 Å radius were fixed. These constraints were kept throughout the remaining simulations. The entire system was weakly coupled[26] to an external heat bath at 300 K with a coupling constant of 0.1 ps and equilibrated for an additional 20 ps.

All the MD and MCTI simulations were then done at constant volume at 300 K with the system coupled[26] to a heat bath. SHAKE[27] was also used with a 2 fs time step. The MCTI was done over 21 windows with 1000 steps of equilibration and 3000 steps of sampling in each window. The total simulation time was 168 ps. A MD simulation of the ADA/DCF complex was done for 100 ps after the equilibration phase. Coordinates were collected every 50 MD steps. Coordinates were also collected every 50 MD steps for 100 ps after the perturbation, with CF bound in the active site.

Inhibitor in Solution. The inhibitor was placed into a box of SPC/E[25] water (30 Å on each side). The initial coordinates for the inhibitor were take from the crystal structure of the ADA/DCF complex. Periodic boundary conditions were employed during relaxation and equilibration. The water was thermalized while the DCF remained fixed. The

DCF was then relaxed and thermalized while the water remained fixed. The DCF and water were weakly coupled to an external heat and pressure bath of 300 K and 10^5 Pa with coupling constants of 0.1 and 0.5 ps, respectively, and equilibrated together for 20 ps. The MCTI simulation was done at constant volume using 1000 steps of equilibration and 2000 steps of sampling in each window over 21 windows for a total of 126 ps. The cutoffs were 9 and 12 Å for the short and long range cutoffs, respectively. The system was coupled[26] to a heat bath using a 0.1 ps coupling constant.

Results and Discussion

The root-mean-square (rms) deviation of the zinc and its bound ligands (His 15, His 17, His 214, Asp 295, and the inhibitor ring) was calculated with respect to the crystal structure at various times during the simulation. The deviations were calculated after equilibration of DCF, after the 100 ps production run with DCF bound in the active site, after the perturbation, and after the 100 ps production run with CF bound in the active site. In each case, the rms deviation was <0.6 Å, which indicates that the model of the zinc and its ligands retains the geometry observed in the crystal structure.

Figure 3 is a stereoview of the DCF molecule bound in the active site of the crystal structure. Also shown are all residues within 6 Å of either C2′ or C3′ of the sugar ring. There are several tight hydrogen bonds between the sugar and other residues of ADA and water. The zinc ligand His 17 is hydrogen bonded to the O5′ of the deoxyribose via the polar hydrogen (Hδ1) of the δ nitrogen (Nδ1). The side chain of Asp 19 hydrogen bonds the HO5′ and the HO3′ of the deoxyribose via Oδ2 and Oδ1, respectively. A crystal water also interacts favorably with the O3′ of the sugar.

Figure 4 is a stereoview of the active site after equilibration but before the perturbation of DCF to CF. All residues within 6 Å of the C2′ or C3′ of the sugar are shown. The zinc ligand His 17 remains hydrogen bonded to the O5′ of the deoxyribose. Asp 19 continues to hydrogen bond with HO5′ through its side chain; however, it now hydrogen bonds with the HO3′ through its carbonyl oxygen. Also the water has moved from the active site, and the O3′ site is now interacting with the hydroxyl hydrogen (HH) of Tyr 68. The ribose ring is near the opening of the active site; thus, the point of perturbation is not within a deep pocket in the protein but at the protein−water interface. Water can enter or leave the opening to the binding site. This snapshot illustrates the mobility of this region of the enzyme−inhibitor complex, as is seen in the simulation.

A ribbon diagram of the ADA crystal structure is shown in Figure 5a along with DCF and the zinc. This orientation gives an overall view of where DCF binds in the active site. Residues 58−67 (helix) and 183−188 (loop) are highlighted in this figure because Wilson et al.[9] have suggested that these residues could possibly serve as lids to the binding site. Motions of these groups will be discussed later. Figure 5b shows the ribbon diagram of the equilibrated structure in the same orientation as the ribbon diagram of the crystal structure (Figure 5a). There is some disorder in residues 58−67 and 183−188, and the inhibitor has moved slightly closer to the helix 58−67. During equilibration, the deoxyribose came into contact with the Phe 65 and Tyr 68, as the water observed in the crystal structure was displaced. The hydroxyl group of the Tyr 68 moved in to satisfy the hydrogen bond contact with the HO3′ that was lost by the displacement of this water.

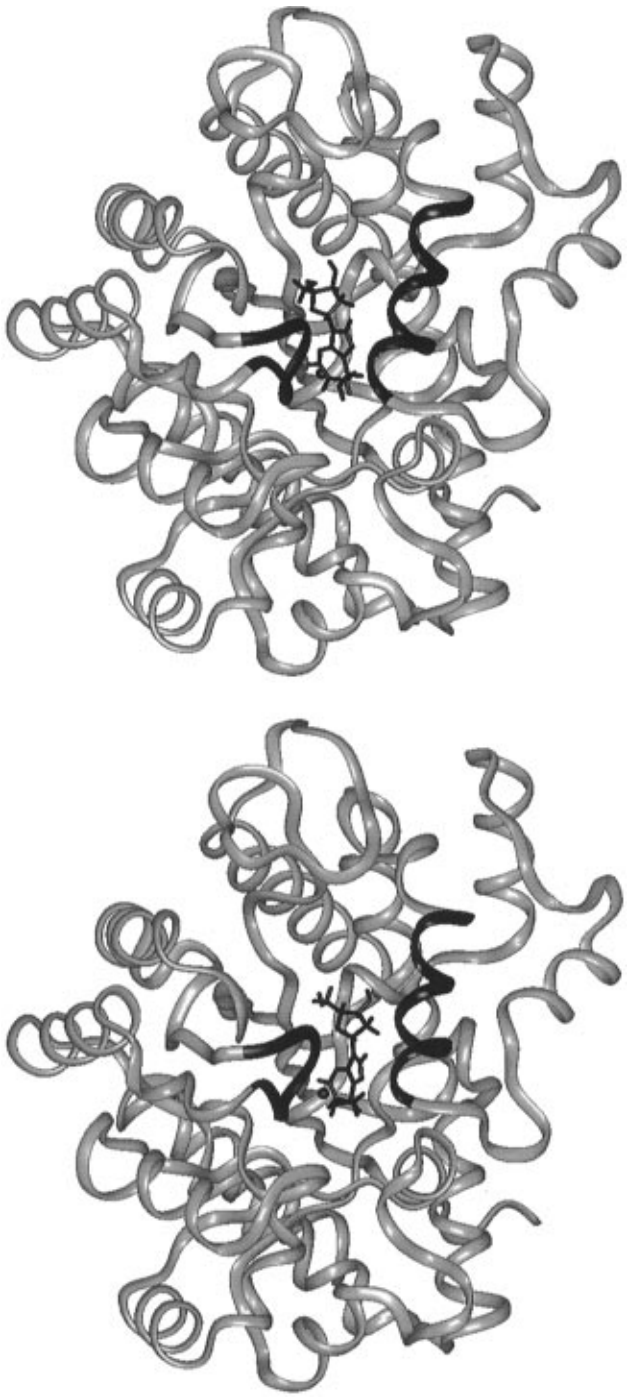

Figure 5. Ribbon diagram (a, top) of the ADA crystal structure and (b, bottom) after equilibration. The zinc and deoxycoformycin are shown to present an overall view of the inhibitor-binding pocket. Helix 58−67 and loop 183−188 are in black.

Table 2. Free Energy Change

mutation	free energy change (kcal/mol)
DCF → CF (in solution)	−12.8 ± 0.3
DCF → (in ADA)	−14.2 ± 0.2
calculated $\Delta\Delta A$	−1.4 ± 0.4
experimental $\Delta\Delta A$	0.8

Table 2 shows the MCTI results for the perturbation of DCF to CF in solution and in the enzyme. The errors reported represent the statistical errors in the individual simulations. Difficulties in obtaining a precise

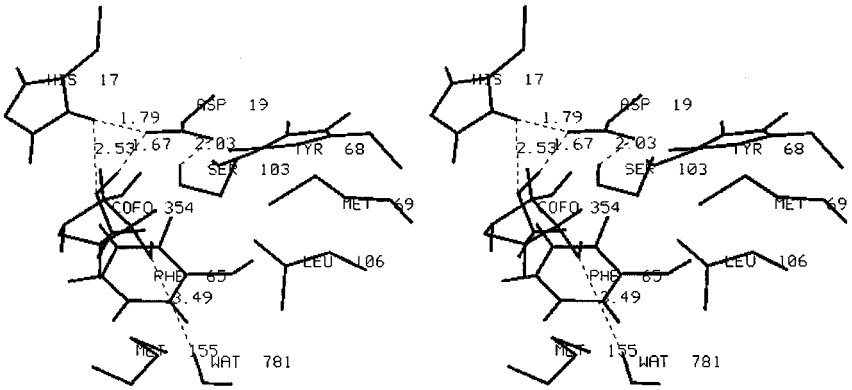

Figure 6. Stereoview of the residues within 6 Å of C2′ or C3′ of coformycin after the mutation from deoxycoformycin to coformycin.

relative free energy of binding can partly be attributed to the high degree of flexibility of the enzyme−inhibitor complex and the free inhibitor, which require sampling over a large number of conformations. The calculated and experimental relative free energies of binding differ in sign. More importantly, however, both are close to zero, showing that the enzyme binds these two inhibitors with similar affinities. Comparison of the dynamic structures of the complexes with the two inhibitors provides insight into the origin of the similarity.

Figure 6 shows a stereoview of the residues within 6 Å of C2′ and C3′ after the perturbation from DCF to CF. Here, Oδ1 of Asp 19 hydrogen bonds with the amide of the backbone of Ser 103 and the hydroxyl hydrogen (Hγ) of the Ser 103 side chain. Asp 19 Oδ2 hydrogen bonds with the HO5′ of CF. The hydrogen bond between His 17 and O5′ lengthens but remains intact during the perturbation. The Hδ1 of His 17 also interacts with Asp 19 Oδ2. During the perturbation, Tyr 68 has moved away from the 2′ position of the sugar to form an interaction with the backbone carbonyl of Asp 19. This backbone carbonyl also forms a hydrogen bond to the HO2′. An intramolecular hydrogen bond is formed between the HO3′ and the O2′ of the CF. A water molecule has moved in to form a long hydrogen bond with O3′. Phe 65 has moved in and is able to form an interaction between its π cloud (represented by the partial charges of the all-atom model for the ring) and the HO3′ of the sugar. Comparing the equilibrated DCF structure in Figure 4 to the perturbed structure in Figure 6, both structures show several schemes of hydrogen bonding. However, the tight bonding between the Hδ1 and His 17 and the O5′ of the sugar ring and between the Asp 19 Oδ2 and the HO5′ of the sugar ring remains constant in both structures. Figure 7 shows a ribbon diagram of ADA and CF bound in the active site after perturbation. This representation shows that ribose has moved away from the residues 58−67, which allows water to interact near the point of perturbation.

The 100 ps trajectories with DCF or CF bound to the enzyme were analyzed to provide additional information on the modes of binding. In particular, the distances between O2′ and O3′ and other residues such as Phe 65 and Tyr 68 were calculated over the trajectories since these interactions are important in the stabilization of the 2′ and 3′ hydroxyl groups. Also the distance between the Hδ1 of His 17 and the O5′ of the sugar was calculated as well as several distances involving groups near the 5′ hydroxyl group of the sugar. The minimum distances, the maximum distances, and the average

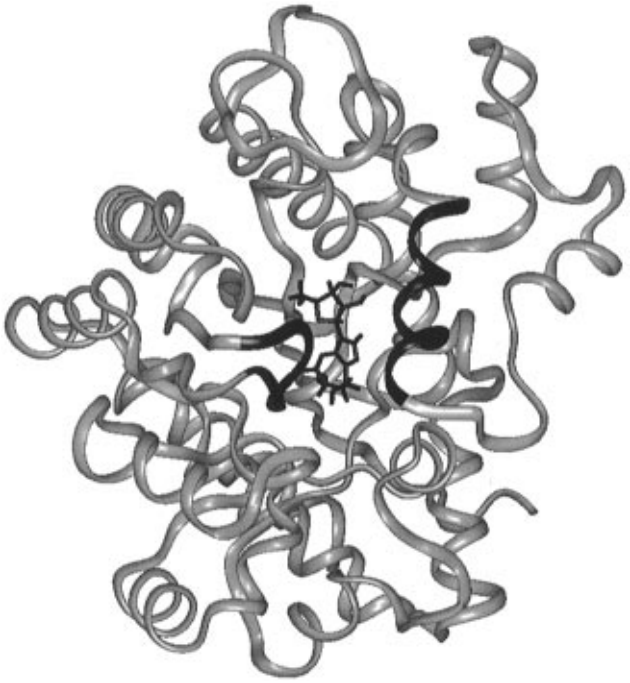

Figure 7. Ribbon diagram of ADA after the mutation. The zinc and coformycin are shown to present an overall view of the inhibitor-binding pocket. Helix 58−67 and loop 183−188 are shown in black.

distance over the 100 ps trajectories of several interactions are summarized in Table 3. From Table 3, it can be seen that there is a strong interaction between Asp 19 and HO5′ with DCF bound in the active site over 100 ps. These interactions are slightly longer during the CF simulation. Phe 65 is in close range of H2′2, a hydrogen of the C2′ group, during the DCF simulation and close to HO3′ during the CF simulation. The average distance between the Hδ1 of His 17 and the O5′ of the sugar is ca. 1 Å longer during the CF simulation than the DCF simulation. Upon close examination of the trajectories, the interaction is lost for a few picoseconds during the CF simulation. At that point the His 17 interacted closely with Asp 19 and the 5′ hydroxyl interacted closely with the side chain of Ser 103. However, the O5′ and the Hδ1 of His 17 moved back into close proximity for the remainder of the simulation. This suggests that the O5′ group of CF is not bound as tightly by His 17 as the O5′ group of DCF and can interact with other protein residues.

Figure 8a,b shows the water hydrogen and water oxygen coordination numbers for the 3′ hydroxyl group of CF averaged over various times during the 100 ps

Table 3. Distances between Active Site Groups during the Deoxycoformycin and Coformycin 100 ps Trajectories

	deoxycoformycin			coformycin		
atom pair	min (Å)	max (Å)	av (Å)	min (Å)	max (Å)	av (Å)
Ser 103 (HN)−Asp 19 (Oδ1)	1.7	3.0	2.3	2.0	5.0	3.5
Ser 103 (HN)−Asp 19 (Oδ2)	1.4	2.4	1.8	1.3	3.5	2.0
Ser 103 (Hγ)−Asp 19 (Oδ1)	1.6	3.9	2.2	1.5	4.6	2.9
Ser 103 (Hγ)−Asp 19 (Oδ2)	1.9	4.7	3.2	1.5	4.5	2.7
Ho5′−Ser 103 (Oγ)	2.4	4.4	3.1	1.6	3.9	3.0
O5′−His 17 (Hδ1)	1.5	2.3	1.8	1.6	5.0	3.0
HO5′−Asp 19 (Oδ1)	1.4	2.2	1.6	1.4	3.8	1.7
HO5′−Asp 19 (Oδ2)	3.0	4.2	3.6	2.2	4.5	3.0
HO3′−Asp 19 (Oδ1)	3.5	5.3	4.4	4.2	6.7	5.1
HO3′−Asp 19 (Oδ2)	4.9	6.7	5.8	4.4	7.2	5.7
HO3′−Asp 19 (O)	1.4	2.1	1.7	3.2	5.9	4.2
HO3′−H2′2/O2′	2.9	3.8	3.4	1.5	3.3	1.9
HO3′−Phe 65 (Cγ)	3.9	6.0	5.0	2.4	4.6	3.4
HO3′−Phe 65 (Cδ1)	4.0	6.7	5.3	2.3	4.2	3.1
HO3′−Phe 65 (Cδ2)	4.0	6.1	5.1	2.3	5.4	3.5
HO3′−Phe 65 (Cϵ1)	4.3	7.1	5.8	2.0	4.8	3.0
HO3′−Phe 65 (Cϵ2)	4.4	6.5	5.6	2.4	5.5	3.5
HO3′−Phe 65 (Cζ)	4.6	6.9	5.9	2.2	4.8	3.3
HO3′−Tyr 68 (OH)	2.8	3.9	3.3	3.4	6.5	5.0
H2′2/O2′−Asp 19 (Oδ1)	6.4	7.6	7.0	3.6	6.3	4.6
H2′2/O2′−Asp 19 (Oδ2)	7.5	9.4	8.6	4.5	7.2	5.7
H2′2/O2′−Phe 65 (Cγ)	2.8	6.1	3.7	3.3	7.1	4.3
H2′2/O2′−Phe 65 (Cδ1)	2.7	6.9	3.9	3.3	6.2	4.4
H2′2/O2′−Phe 65 (Cδ2)	2.4	4.9	3.1	3.1	6.3	3.8
H2′2/O2′−Phe 65 (Cϵ1)	2.6	6.7	3.7	2.9	6.2	4.1
H2′2/O2′−Phe 65 (Cϵ2)	2.3	4.7	2.9	2.8	6.1	3.5
H2′2/O2′−Phe 65 (Cζ)	2.3	5.5	3.2	2.8	5.2	3.6
HO2′−Asp 19 (Oδ1)				2.9	5.8	4.3
HO2′−Asp 19 (Oδ2)				4.0	6.7	5.3
HO2′−Asp 19 (O)				1.6	4.7	2.1
HO2′−O3′				1.5	3.6	3.1
HO2′−Phe 65 (Cγ)				3.4	5.6	4.5
HO2′−Phe 65 (Cδ1)				3.4	6.0	4.9
HO2′−Phe 65 (Cδ2)				3.0	5.1	4.0
HO2′−Phe 65 (Cϵ1)				2.8	6.2	4.8
HO2′−Phe 65 (Cϵ2)				2.8	5.4	3.9
HO2′−Phe 65 (Cζ)				2.5	5.5	4.3
HO2′−Tyr 68 (OH)				2.2	5.2	3.9
O3′−Tyr 68 (HH)	1.5	2.7	1.8	3.9	7.1	5.5
O2′−Tyr 68 (HH)				2.9	5.9	4.1
Tyr 68 (HH)−Asp 19 (O)	2.8	4.4	3.7	1.6	4.3	2.5

trajectory, respectively. Between the times of 20 and 40 ps during the 100 ps simulation, one water is within hydrogen-bonding distance of the 3′ hydroxyl group. At other times, there is on average less than one water within hydrogen-bonding distance. This indicates that water moves in and out of hydrogen-bonding distance of the 3′ group during the simulation. In particular, water can more closely approach O3′ than the HO3′ of the hydroxyl group because the HO3′ is engaged in a close interaction with O2′. However, no waters were within hydrogen-bonding distance of the 2′ group of CF or the 3′ group of DCF; thus corresponding plots are not shown for these groups.

Figures 9 and 10 show stereoviews of the final structures after the 100 ps trajectory of DCF and the 100 ps trajectory of CF. Again, residues within 6 Å of C2′ or C3′ are shown. During the simulation with DCF bound to ADA, water moved in to hydrogen bond with the O1′ of the sugar. The hydrogen bond network at the 5′ position is similar to the network of the equilibrated structure in Figure 4. During the CF simulation, a water came into hydrogen-bonding distance of the ribose O3′. However, no water is within hydrogen-bonding distance of the 2′ hydroxyl group. The proton of the HO3′ group of ribose interacts favorably with the π cloud of Phe 65. Asp 19 is part of an intricate array

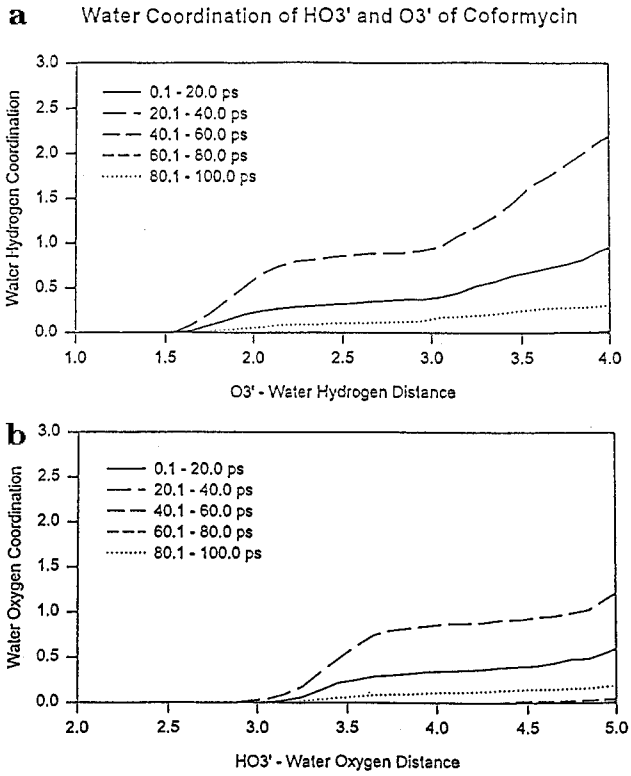

Figure 8. (a) Water hydrogen and (b) water oxygen coordination of the coformycin 3′ hydroxyl group averaged over 20 ps blocks of time during the 100 ps trajectory.

of hydrogen bonding and close contacts with Ser 103, His 17, and the 5′ sugar hydroxyl as is also seen in Figure 5.

Although a much more extensive simulation would need to be done to examine flexibility of the loops of the enzyme, rms deviations from the crystal structure were measured for all atoms at the end point conformations of the 100 ps trajectories. The rms deviations were obtained by translating and rotating the entire protein (without the inhibitor) to give the best overall fit. The rms deviations from the crystal structure with DCF bound in the active site range from 1.0 to 3.4 Å for residues 58−67 and 0.5 to 2.5 Å for residues 183−188, which may serve as lids[9] to the binding pocket. The rms deviations from the crystal structure with CF bound in the active site range from 1.2 to 3.2 Å for residues 58−67 and 0.5 to 2.5 Å for residues 183−188. The rather modest difference in the free energy of binding of the two inhibitors is in part due to the fact the 2′ and 3′ hydroxyl groups are not tightly sequestered within the protein environment. The solvent molecules and loop residues can rearrange fairly easily to have favorable interactions with the sugar 2′ and 3′ hydroxyl groups.

Conclusions

A force field model was developed to describe the ADA active site. Although this bonded model is not designed to describe perturbations at the zinc center itself, it has the flexibility necessary to allow for structural changes associated with the perturbation of DCF to CF. Since DCF and CF differ by a hydroxyl group, one might imagine that the relative free energy of binding would be larger than 1 kcal/mol if the 2′ position were sequestered in a hydrophobic pocket. However, the 2′

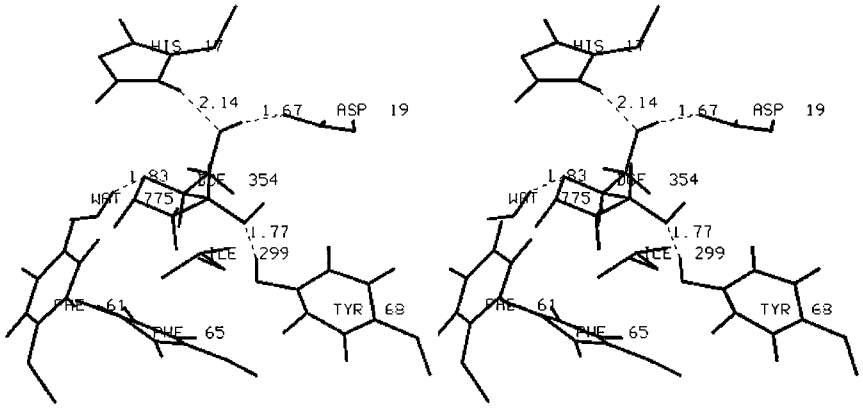

Figure 9. Stereoview of all residues within 6 Å of C2′ or C3′ of deoxycoformycin at the end point of the 100 ps trajectory.

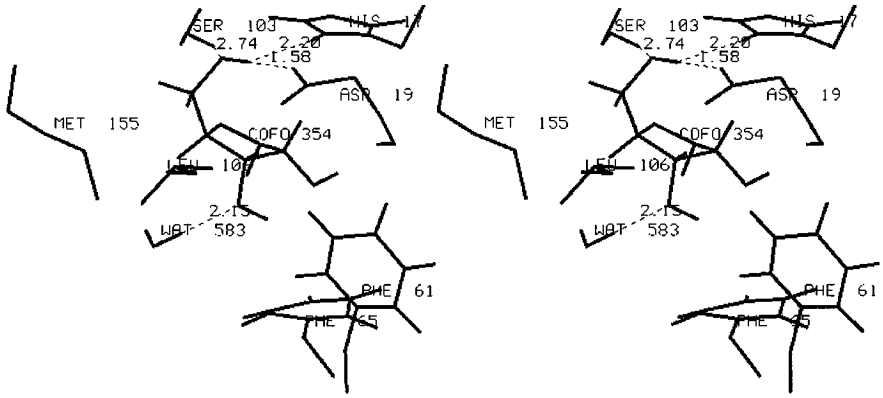

Figure 10. Stereoview of all residues within 6 Å of C2′ or C3′ of coformycin at the end point of the 100 ps trajectory.

position is at the opening of the active site, which allows for facile water penetration and interaction of the inhibitors with a variety of residues at the opening. This flexibility accounts for the ability of the enzyme to accommodate either inhibitor. It also makes it difficult to define the relative free energy of binding very precisely, due to the need to average over a large number of configurations of the inhibitor−enzyme complex.

The MD simulation of CF bound in the active site showed a favorable interaction of the Phe 65 ring with the 3′ hydroxyl group. This is interesting because it is an example of an aromatic behaving as a weak hydrogen bond acceptor.[28] Asp 19 has been shown to be a key residue in the sequestering of the sugar in the pocket by forming intricate hydrogen-bonding networks with the sugar hydroxyl groups in both simulations. His 17 was also shown to be a tight binder of the 5′ hydroxyl group in both simulations. Mutations at these protein sites could have severe consequences on the binding of CF or DCF. The 5′ hydroxyl group is in a sequestered environment compared to the environments of the 2′ and 3′ hydroxyl groups. Due to its strong interactions with His 17 and Asp 19, removal of the 5′ hydroxyl group of the inhibitor could have profound effects on the binding of these transition-state-like inhibitors.

Acknowledgment. We would like to thank Dr. J. Tirado-Rives for providing us with OPLS parameters for all-atom aromatic residues and Biosym for the InsightII software used to generate the stereoviews. This research was supported in part by NSF and SDSC. T.J.M. is an NIH postdoctoral fellow. F.A.Q. is an investigator of the Howard Hughes Medical Institute.

Supporting Information Available: Bond, angle, and dihedral parameters used in the active site force field (1 page). Ordering information is given on any current masthead page.

References

(1) Kredich, N. M.; Hershfield, M. S. In *The Metabolic Basis of Inherited Disease*; Scrivner, R., et al., Eds.; McGraw-Hill: New York, 1989; Vol. 6, pp 1045−1075.
(2) Goodchild, J. The Biochemistry of Nucleoside Antibiotics. In *Topics in Antibiotic Chemistry*; Sammes, P. G., Ed.; John Wiley & Sons: New York, 1982; Vol. 6, pp 99−227.
(3) Barchi, J. J., Jr.; Marquez, V. E.; Driscoll, J. S.; Ford, H., Jr.; Mitsuya, H.; Shirasaka, T.; Aoki, S.; Kelly, J. Potential Anti-AIDS Drugs. Lipohilic, Adenosine Deaminase-Activated Prodrugs. *J. Med. Chem.* **1991**, *34*, 1647−1655.
(4) Ford, H., Jr.; Siddiqui, M. A.; Driscoll, J. S.; Marquez, V. E.; Kelley, J. A.; Mitsuya, H.; Shirasaka, T. Lipohilic, Acid-Stable, Adenosine-Deaminase-Activated Anti-HIV Prodrugs for Central Nervous System Delivery. 2. 6-Halo and 6-Alkoxy Prodrugs of 2′-B-Fluoro-2′,3′-dideoxyinosine. *J. Med. Chem.* **1995**, *38*, 1189−1195.
(5) Cha, S.; Agarwal, R. P.; Parks, R. E., Jr. Tight-Binding Inhibitors-II Non-Steady State Nature of Inhibition of Milk Xanthine Oxidase by Allopurinol and Alloxanthine and of Human Erythrocytic Adenosine Deaminase by Coformycin. *Biochem. Pharmacol.* **1975**, *24*, 2187−2197.
(6) Agerwal, R. P.; Spector, T.; Parks, R. E., Jr. Tight-Binding Inhibitors-IV Inhibition of Adenosine Deaminases by Various Inhibitors. *Biochem. Pharmacol.* **1977**, *26*, 359−367.
(7) Wolfenden, R.; Wentworth, D. F.; Mitchell, G. N. Influence of Substituent Ribose on Transition State Affinity in Reactions Catalyzed by Adenosine Deaminase. *Biochemistry* **1977**, *16*, 5071−5077.
(8) Wilson, D. K.; Quiocho, F. A. Unpublished results.
(9) Wilson, D. K.; Rudolph, F. B.; Quiocho, F. A. Atomic Structure of Adenosine Deaminase Complexed with a ransition State Analog: Understanding Catalysis and Immunodeficiency Mutations. *J. Chem. Phys.* **1991**, *91*, 3631−3637.
(10) Frisch, M. J.; Trucks, G. W.; Head-Gordon, M.; Gill, P. M. W.; Wongand, M. W.; Foresman, J. B.; Johnson, B. G.; Schlegel, H. B.; Robb, M. A.; Replogle, E. S.; Gomperts, R.; Andres, J. L.; Raghavachari, K.; Binkley, J. S.; Gonzalez, C.; Martin, R. L.; Fox, D. J.; Defrees, D. J.; Baker, J.; Stewart, J. J. P.; Pople, J. A. *Gaussian92, Revision E.2*; Gaussian Inc.: Pittsburgh, PA, 1992.

(11) Dunning, J.; Hay, P. J. In *Methods of Electronic Structure Theory*; Schaeffer, H. F., III, Ed.; Plenum Press: New York, 1977; pp 1−28.
(12) Hay, P. J.; Wadt, W. R. Ab initio Effective Core Potentials for Molecular Calculations. Potentials for the Transition Metal Atoms Sc to Hg. *J. Chem. Phys.* **1985**, *82*, 270−283.
(13) Breneman, C. M.; Wiberg, K. B. Determining Atom-centered Monopoles from Molecular Electrostatic Potentials- The Need for High Sampling Density in Formamide Conformational Analysis. *J. Comput. Chem.* **1990**, *11*, 361.
(14) Hoops, S. C.; Anderson, K. W.; Merz, K. M., Jr. Force Field Design of Metalloproteins. *J. Am. Chem. Soc.* **1991**, *113*, 8262−8270.
(15) Jorgensen, W. L. *BOSS 31*. Yale University: New Haven, CT, 1991.
(16) Jorgensen, W. L.; Tirado-Rives, J. The OPLS Potential Functions for Proteins. Energy Minimizations for Crystals of Cyclic Peptides and Crambin. *J. Am. Chem. Soc.* **1988**, *110*, 1657−1666.
(17) Weiner, S. J.; Kollman, P. A.; Nguyen, D. T.; Case, D. A. An All Atom Force Field for Simulation of Proteins and Nucleic Acids. *J. Comput. Chem.* **1986**, *7*, 230−252.
(18) Tirado-Rives, J. Personal communication.
(19) Smith, P. E.; Dang, L. X.; Pettitt, B. M. Simulation of the Structure and Dynamics of the Bis(Penicillamine) Enkephalin-Zwitterion. *J. Am. Chem. Soc.* **1991**, *113*, 67−73.
(20) Antosiewicz, J.; McCammon, J. A.; Gilson, M. K. Prediction of PH-Dependent Properties of Proteins. *J. Mol. Biol.* **1994**, *238*, 415−436.
(21) Davis, M. E.; Madura, J. D.; Luty, B. A.; McCammon, J. A. Electrostatics and Diffusion of Molecules in Solution with the University of Houston Brownian Dynamics Program. *Comput. Phys. Commun.* **1991**, *62*, 187−197.
(22) Straatsma, T. P.; McCammon, J. A. Computational Alchemy. *Annu. Rev. Phys. Chem.* **1992**, *43*, 407−435.
(23) Straatsma, T. P.; McCammon, J. A. Multiconfiguration Thermodynamic Integration. *J. Chem. Phys.* **1991**, *91*, 3631−3637.
(24) Straatsma, T. P.; McCammon, J. A. Argos, A Vectorized General Molecular Dynamics Program. *J. Comput. Chem.* **1990**, *11*, 943−951.
(25) Berendsen, H. J. C.; Grigera, J. R.; Straatsma, T. P. The Missing Term in Effective Pair Potentials. *J. Phys. Chem.* **1987**, *91*, 6269.
(26) Berendsen, H. J. C.; Postma, J. P. M.; van Gunsteren, W. F.; DiNola, A.; Haak, J. R. Molecular Dynamics with Coupling to an External Heat Bath. *J. Chem. Phys.* **1984**, *81*, 3684.
(27) Ryckaert, J. P.; Ciccotti, G.; Berendsen, H. J. C. Numerical Integration of the Cartesian Equations of Motion of a System with Constraints: Molecular Dynamics of n-Alkanes. *J. Comput. Phys.* **1977**, *23*, 327.
(28) Suzuki, S. S.; Green, P. G.; Bumgarner, R. E.; Dasgupta, S.; Goddard, W. A., III; Blake, G. A. Benzene Forms Hydrogen Bonds with Water. *Science* **1992**, *257*, 942−945.

JM9505674